ISSN 1392–1320 MATERIALS SCIENCE (MEDŽIAGOTYRA). Vol. 13, No. 4. 2007

Probe Temperature Measurements and Optical Emission Spectroscopy in Vacuum Plasma Spraying Process Control

Tomas GRINYS[1,2*], Sigitas TAMULEVIČIUS[1,2], Irmantas MOCKEVIČIUS[1,2], Mindaugas ANDRULEVIČIUS[2]

[1]*Physics Department, Kaunas University of Technology, Studentu 50, LT-51368 Kaunas, Lithuania*
[2]*Institute of Physical Electronics of Kaunas University of Technology, Savanoriu 271, LT-50131 Kaunas,* Lithuania

Received 24 September 2007; accepted 11 October 2007

The investigations on a vacuum plasma spray process under different H_2/Ar working gas flow without and with powder injection were carried out. The tungsten probe was placed inside the vacuum chamber and it's temperature was evaluated by means of the optical pyrometer. The factorial orthogonal central composite experimental plan design allowed us to get an empirical equation of the probe temperature distribution in the plasma torch for 25 l/min – 31 l/min and 4 l/min – 8 l/min interval of Ar and H_2 gas flow respectively. To study the processes occurring in vacuum plasma spraying the optical emission spectroscopy has been employed as well. The optical emission spectrum consisted of hydrogen Balmer series and excited argon lines before the powder injection into the plasma. After injection of YSZ, NiO powder mixture into the plasma, the sharp peaks appeared in the wavelength range of 380 nm – 480 nm. The correlation between the deposition rate of the vacuum plasma spray process and the integrated intensity in the wavelength range of 380 nm – 480 nm of optical emission spectrum was examined in the present work.
Keywords: vacuum plasma spray, YSZ, NiO, Ni, probe, optical emission spectroscopy.

INTRODUCTION

Plasma spraying technologies are widly used to deposit a considerable variety of composite ceramic coatings. High temperatures and deposition rates are common in plasma spraying process. The spray process is based on the generation of a plasma jet consisting of argon or argon with admixtures, which are ionized by high current arc discharge inside a plasma torch. The powders to be sprayed are injected into the plasma, where they are accelerated, melted and finally deposited onto the substrate [1].

In order to get well melted injected particles and good quality, controlled thickness coatings, it is convenient to ensure control of plasma spray parameters such as plasma flame/injected particle temperature and velocity [2, 3]. Several in situ plasma diagnostic tools exist to determine the plasma torch temperature. One of the most spread is optical emission spectroscopy (OES). This method is based on the spectral analysis of optical radiation emitted by excited atoms or molecules then they return to the lower energy state level. OES has been successfully applied to identify the species present in the plasma .The difficulties in estimating the plasma temperature one can find then spraying process is performed in a vacuum. Such plasma is not in the thermodynamic equilibrium [4] and the temperature of it must be expressed by excited neutrals, ions and electrons temperatures (T_{exc}, T_{ion}, T_e). Calculating T_{exc}, T_{ion}, T_e separately is a difficult and much time demanding task [5].

In the case of non-equilibrium plasma it is more convenient to investigate the overall energy of neutrals, ions and electrons transferred to the probe placed inside a plasma torch. The simplicity of equipment and experiment constitute the advantages of the probe method [6]. The main limitation of this method is that it is an intrusive method, causing a local perturbation of the plasma [7].

The present work aims at a diagnostics of the plasma torch under different Ar/H_2 working gas flow ratio before and after powder injection. The factorial experimental plan was applied to get an empirical probe temperature dependence on Ar/H_2 gas flow. The OES spectra were analyzed for getting information about the processes occurring in a plasma jet. The vacuum plasma spray equipment in this work was employed to produce YSZ-NiO-Ni (yttria stabilized zirconia, nickel oxide, nickel) coatings. YSZ-NiO-Ni cermet remains promising solid anode material for use in solid oxide fuel cells, consisting of an anode, a YSZ electrolyte and a $La_{1-x}SrMnO_3$ cathode [8].

EXPERIMENTAL

The equipment used for the plasma generation and deposition of YSZ-NiO-Ni coatings consists of a commercially available plasma gun (SG-100 Miller Thermal Inc.) mounted in a water-cooled vacuum chamber, cooling substrate holder and computerized powder feeder (Fig. 1). Argon and hydrogen were as a primary and a secondary working gas for plasma jet respectively. A rotor vacuum pump allowed maintaining 1153 Pa – 1360 Pa pressure in the chamber. The plasma spray parameters used during the experiment are given in Table 1.

The probe used for the plasma torch diagnostics was made of a tungsten stick (2 mm in diameter). The naked top part of it was exposed to the plasma and the bottom part was wrapped in an alumina insulator to ensure a good thermal resistance. The temperature of the heated probe was measured at a constant distance of 25 cm from the plasma gun nozzle by the optical pyrometer LOP-72 with a filter for a wavelength $\lambda = 650$ nm. It is known from

*Corresponding author. Tel.: +370-37-313432; fax.: +370-37-314423.
E-mail address: *Tomas.Grinys@stud.ktu.lt* (T. Grinys)

literature [9], that plasma torch has steep temperature gradients not only in the axial but in the radial direction also. Therefore, the point at the hottest part of the probe was measured at the point corresponding to the centre of plasma torch.

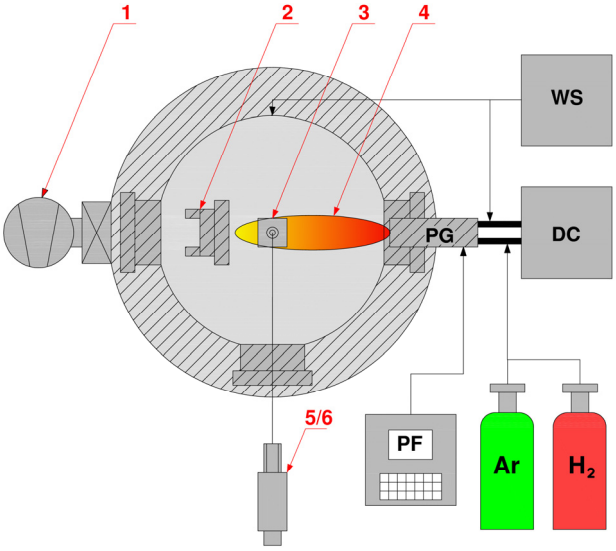

Fig. 1. Schematic diagram of the experimental setup: PG – plasma gun (SG-100 Miller Thermal), WS – water supply system, DC – DC power source, PF – computerized powder feeder, 1 – vacuum pump, 2 – cooling substrate holder, 3 – tungsten probe, 4 – plasma torch, 5 / 6 – pyrometer / spectrometer

Table 1. Vacuum plasma spray processing parameters

Current	500 A – 640 A
Voltage	27 V – 35 V
Primary gas Ar	25 l/min – 31 l/min
Secondary gas H_2	4 l/min – 8 l/min
Powder feed rate	10 g/min – 20 g/min
Standoff distance	30 cm
Pressure in the chamber	1049 Pa – 1330 Pa

An optical spectrometer of AvaSpec design was used to the get a plasma spectrum in the range of 300 nm – 1000 nm. The spectrum below 400 nm was partly filtered, because the spectrometer was separated from the plasma radiation by a vacuum chamber window made of glass. The light entering a spectroscopic system was collimated by the spherical mirror, diffracted by the plane grating 300 lines/mm and focused by the second spherical mirror to the 2048 pixel CCD detector. The spectrometer has a wavelength depth resolution of 1.4 nm.

RESULTS AND DISCUSSION

Influence of the Ar/H_2 working gas flow rate on the plasma torch length and shape was examined firstly. Fig. 2. shows the plasma jet pictures under different working gas flow rate. After Ar gas flow has been increased from 25 l/min to 31 l/min (totally flow rate has been increased from 29 l/min to 35 l/min) the plasma torch suffered a contraction in the axial and an expansion in the radial direction. The experimental results showed the same effect with the increased hydrogen gas flow rate. This is due to transition of the plasma spray regime. When gas flow increases an interaction between the adjacent plasma jet layers and the surrounding cold particles becomes stronger leading to a gas mixing. Thus the quasi-laminar plasma jet transforms into the turbulent one. Following the experimental results found in the literature [9], temperature gradients of the laminar plasma jets with long plasma torches in axial direction are about two orders lower then those of the turbulent plasma jets. That means, one can expect a lower temperature of the plasma torch at a constant distance from nozzle with a higher gas flow rate.

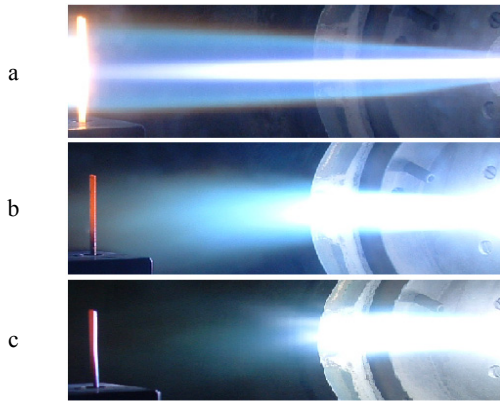

Fig. 2. Pictures of the plasma jet torches at a different Ar/H_2 working gas flow rate: a – Ar/H_2 flow rate is 25/4 l/min (pressure 1153 Pa), b – Ar/H_2 flow rate is 28/4 l/min (pressure 1074 Pa), c – Ar/H_2 flow rate is 31/4 l/min (pressure 1126 Pa). The probes on the left side of figures placed at distances of 25 cm from plasma gun

Further diagnostics on the plasma torch have been made by the tungsten probe. The top part of it is shown on the left side of Fig. 2. In all cases the probe temperature measurements were done after 30 s exposition in the plasma when equilibrium conditions have been reached. The spectral emissivity of tungsten at a wavelength 650 nm was expressed by the first order polynomial $\varepsilon_\lambda(T) = 0.478 - 2\cdot10^{-5}T$ in the temperature range of 1000 K – 2800 K [10] and the equation used for the tungsten temperature calculation

$$T = \frac{CT_b}{C + \lambda T_b \ln \varepsilon_\lambda} \qquad (1)$$

was derived from Planks law. The constant C in Eq. (1) is equal $C = hc / k$, h is the Plank constant, c is the speed of light, k is the Boltzmann constant, T_b is the temperature measured by the pyrometer. Spectral emissivity in Eq. 1 is a function of temperature that is the object of calculations, therefore Solver utility of Microsoft Excel was used to find the best fitted value of T.

The factorial orthogonal central composite plan design [11, 12] was chosen to obtain the probe temperature distribution under different Ar/H_2 gas flow rate. Each of two normalized plasma spray parameters was varied between low (–1), main (0) and high (+1) level independently. The transition between real and normalized x_1, x_2 variables can be made on the basis of the following relationships:

$$x_1 = \frac{F_{H_2} - 6}{2}; \quad x_2 = \frac{F_{Ar} - 28}{3}, \qquad (2)$$

where F_{H_2} and F_{Ar} are the hydrogen and argon gas flow rates (l/min) respectively. Totally 9 experiments are necessary to run over all treatment combinations x_1, x_2. In order to estimate the accuracy of temperature measurements and adequacy of the model the experiments were repeated twice. The planning matrix, the average measured temperatures of the probe heated by the plasma (T_E) are presented in Table 2. The influence of the process parameters F_{H_2}, F_{Ar} on probe temperature placed in the plasma was described mathematically by the second order regression equation. After the calculations have been made on the coefficients of regression equation, the probe temperature dependence on hydrogen and argon gas flow rates was found to be:

$$T(F_{H_2},F_{Ar}) = 7167.62 + 72.33F_{H_2} - 282.33F_{Ar} - \\ -26.94F_{H_2}^2 + 2.18F_{Ar}^2 + 9.43F_{H_2}F_{Ar} \quad . \qquad (3)$$

The last column in Table 2 shows the calculated temperature values by Eq. (3) for the comparison. The adequacy of the introduced mathematical model was checked by the Fisher's criteria with a significance level of 0.05. The value of R^2 was calculated also. According to the Fisher's criteria the mathematical model of the experiment can be accepted, because requirement for such criteria was fulfilled (calculated Fisher's coefficient was less then tabulated: $F_{calc} < F_{tab}$ i. e. $2.69 < 3.37$). It should be mentioned that calculated R^2 for Eq. (3) is 0.986.

Table 2. The factorial orthogonal central composite experimental plan design

No.	Treatment combination		Average values	Calculated values
	x_1	x_2	T_E, K	T, K
1	1	–1	2196	2212
2	1	1	1663	1703
3	–1	1	1535	1537
4	–1	–1	2295	2273
5	1	0	1993	1938
6	–1	0	1867	1885
7	0	1	1771	1728
8	0	–1	2344	2350
9	0	0	1983	2019

The graphical view of the argon/hydrogen flow rate influence on probe temperature expressed by equation (3) is shown in Fig. 3. A higher Ar gas flow rate results in a lower enthalpy of the ionized Ar/H_2 gas mixture. Furthermore, the experiments on plasma torch shape described previously showed contraction of plasma torch in axial direction, when gas flow rate was increased. Both effects lead to the probe temperature decrease.

For the increased H_2 gas flow rate, the probe temperature variation was different (Fig. 3). There was observed an existence of the maximum temperature value. Such distribution of the probe temperature can be explained by competition of two effects: the high enthalpy of the ionized H_2 gas leading to the temperature increase and transition of the plasma torch regime from quasi-laminar to the turbulent one leading to the decrease of temperature.

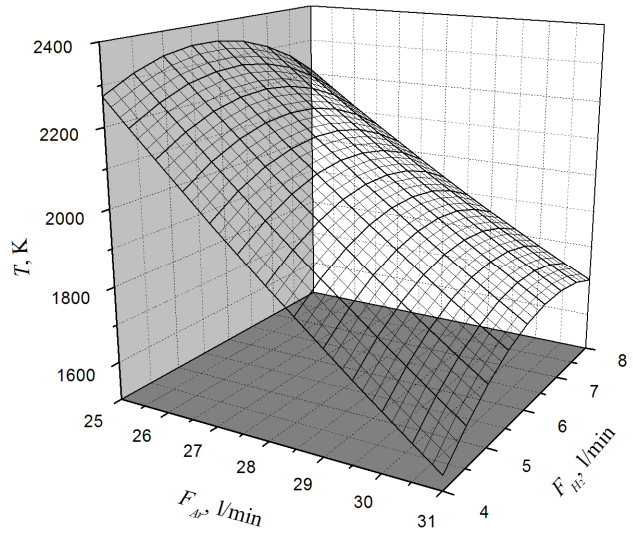

Fig. 3. Probe temperature v. s. argon F_{Ar} and hydrogen F_{H_2} working gas flow rate. The probe was kept in the vacuum chamber at a constant distance of 25 cm from the plasma gun. The power of an arc discharge varied in the range of 17.4 kW (voltage 30 V, current 580 A) and 19.2 kW (voltage 30 V, current 640 A)

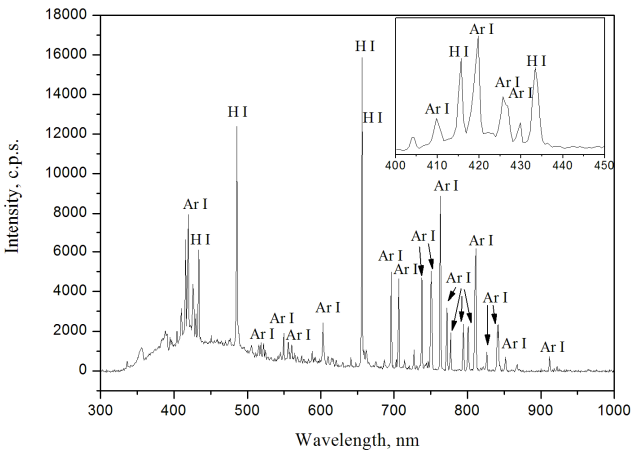

Fig. 4. Optical emission spectrum of the arc discharge plasma. Ar and H_2 was used as a primary and a secondary working gas

To investigate the processes occurring in the vacuum plasma spraying the OES has been employed as well. The emission spectra consisted of hydrogen Ballmer series (H I) and excited argon (Ar I) lines (before powder injection into the plasma) (Fig. 4). The relative intensities of un-overlapped hydrogen (wavelength 486 nm) and argon (wavelength 763 nm) peaks I_H/I_{Ar} were studied as a function of the hydrogen and argon working gas flow rate. The regression equation Eq. (4) was obtained in the same manner as described above.

$$I_H / I_{Ar}(F_{H_2},F_{Ar}) = 8.86 + 1.58F_{H_2} - 0.63F_{Ar} - \\ -0.09F_{H_2}^2 + 0.01F_{Ar}^2 - 0.01F_{H_2}F_{Ar} \quad . \qquad (4)$$

Calculated R^2 in this case for Eq. (4) is 0.984.

The plot of Eq. (4) is given in Fig. 5. The values of relative intensities I_H/I_{Ar} (Fig. 5) show an increase with increased H_2 flow and decrease with increased Ar flow corresponding to the rate of excitation and ionization of the working gas mixture. Similar variation of the intensities ratios was found for all un-overlapped Ar I and H I peaks.

At higher H_2 content in Ar/H_2 gas mixture one can expect higher probe temperature placed in the plasma because of higher enthalpy of ionized H_2 gas as compared with Ar. However, different distributions of probe temperature and values of relative intensities I_H/I_{Ar} v. s. Ar/H_2 gas flow rate confirm the fact of competition of several processes and existence of the optimal plasma spray regime.

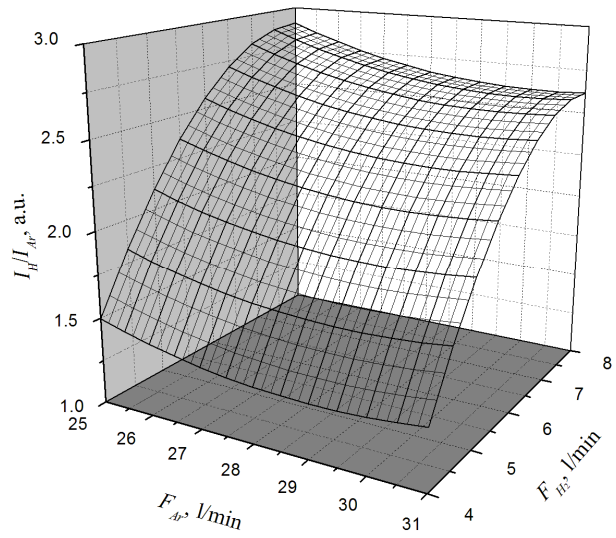

Fig. 5. Excited hydrogen ($\lambda = 486$ nm) and argon ($\lambda = 763$ nm) lines intensities ratio I_H/I_{Ar} v. s. argon F_{Ar} and hydrogen F_{H_2} working gas flow rate. The power of arc discharge varied in the range of 17.4 kW (voltage 30 V, current 580 A) and 19.2 kW (voltage 30 V, current 640 A)

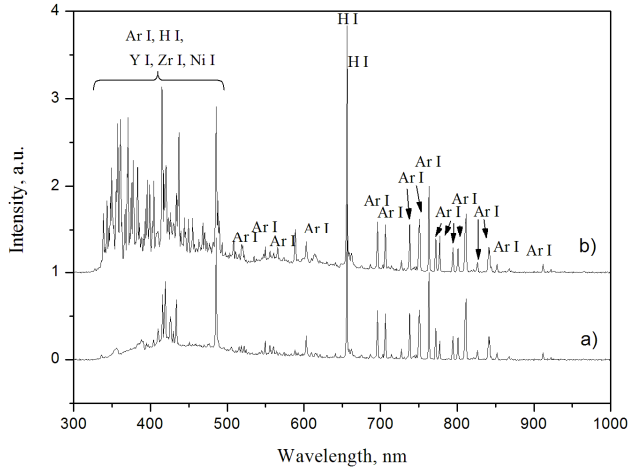

Fig. 6. Spectrum of the arc discharge plasma: a – before and after b – YSZ – NiO powder injection

The experiments at a different Ar/H_2 working gas flow rate were performed with powder injection into the plasma. The sharp peaks appeared in the wavelength range of 380 nm – 500 nm after injection of YSZ, NiO powder mixture into the plasma (Fig. 6). The optical emission spectrum peaks were compared with the catalogue data of the corresponding element emission lines. These lines can be assigned to the excited and ionized Y, Zr, Ni atoms [10]. The optical emission spectrum intensity after powder injection was normalized with regard to the most intensive Ar I line at a wavelength of 763 nm. It was observed that integrated intensity in the 380 nm – 500 nm wavelength range of the normalized spectrum was varying because of chosen different plasma spray parameters such as Ar/H_2 working gas flow rate and powder injection speed rate.

The correlation between the deposition rate of coatings formed by vacuum plasma spray process and the integrated intensity of the normalized spectrum in the 380 nm – 500 nm wavelength range was found. The plot of the deposition rate as a function of integrated intensity is shown in Fig. 7.

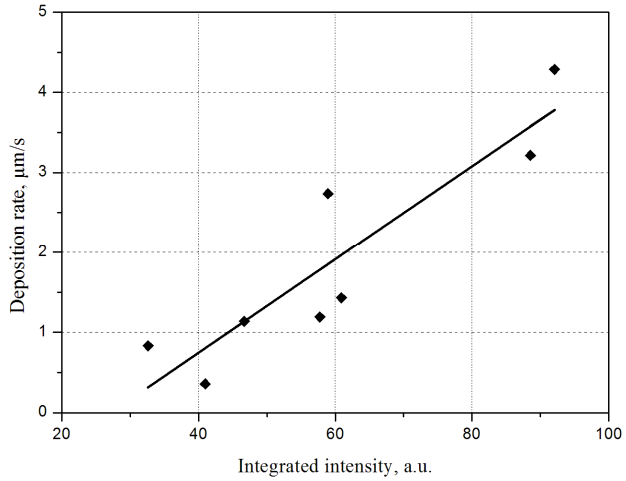

Fig.7. Deposition rate of coatings formed by vacuum plasma spray as a function of integrated intensity of emission lines in the wavelength range of 380 nm – 500 nm

The deposition rate increases with increase of the integrated intensity and seems to be almost proportional to it ($R^2 = 0.824$ of the trend line). This experimental result can be used for control of the coatings deposition. However the deviations from the linear dependence are observed particularly at high deposition rates, therefore the point corresponding to treatment combination No. 2 (Table 2) was rejected. These deviations can be caused by spontaneous spray instability as well as by processes such as dissociation of powder in the plasma that lead to indirect excitation and ionization of the atoms. The spectrum itself in the wavelength range of 380 nm – 500 nm still contains Ar I and H I emission lines. This can be a reason as well of the deflection from the linear dependence.

CONCLUSIONS

A diagnostics of the vacuum plasma spray process was performed by probe and OES method under different Ar/H_2 working gas flow. It was found that two effects influence the change of the probe temperature mainly. At a higher H_2 content in Ar/H_2 gas mixture the probe temperature increases because of higher enthalpy of the ionized H_2 gas as compared with Ar. When the total gas flow is too high quasi-laminar plasma torch transforms into turbulent one leading to the probe temperature decrease.

The competition between these two effects results an existence of the probe temperature maximum and optimal vacuum plasma spray regime.

The analysis of optical emission spectrum revealed that the ionized Ar/H_2 gas mixture emission lines consisted of H I Ballmer series and excited Ar I lines in the wavelength range of 380 nm – 800 nm before powder injection into the plasma. The sharp peaks appeared in the wavelength range of 380 nm – 500 nm after injection of YSZ, NiO powder mixture into the plasma. These lines can be assigned to the excited and ionized Y, Zr, Ni atoms.

The integrated intensity in the 380 nm – 500 nm wavelength range of the normalized emission spectrum after powder injection as well as deposition rate of coatings were sensitive to the chosen different plasma spray parameters. It was found linear dependence between the deposition rate and intensity of integrated optical emission at low deposition rate.

REFERENCES

1. **Will, J., Mitterdorfer, A., Kleinlogel, C., Perednis, D., Gauckler, L. J.** Fabrication of Thin Electrolytes for Second-Generation Solid Oxide Fuel Cells *Solid State Ionics* 131 2000: pp. 79 – 96.
2. **Heimann, R. B.** Plasma-Spray Coating. VCH, 1996: 339 p.
3. **Friis, M., Persson, C., Wigren, J.** Influence of Particle In-flight Characteristics on the Microstructure of Atmospheric Plasma Sprayed Yttria Stabilized ZrO_2 *Surface & Coatings Technology* 2001: pp. 115 – 127.
4. **Pawlowski, L.** The Science and Engineering of Thermal Spray Coatings. Wiley, 1995: 372 p.
5. **Garcı´a, L. A., Restrepo, E., Jime´nez, H., Castillo, H. A., Ospina, R., Benavides, V., Devia, A.** Diagnostics of Pulsed Vacuum Arc Discharges by Optical Emission Spectroscopy and Electrostatic Double-Probe Measurements *Vacuum* 81 2006: pp. 411 – 416.
6. **Raizer, Y. P.** Gas Discharge Physics. Springer, 1997: 449 p.
7. **Chen, W. L. T., Heberlein, J., Pfender, E.** Diagnostics of a Thermal Plasma Jet by Optical Emission Spectroscopy and Enthalpy Probe Measurements *Plasma Chemistry and Plasma Processing* 1994: pp. 317 – 332.
8. **Rojas, A. R., Esparza-Ponce, H. E., Fuentes, L., L´opez-Ortiz, A., Keer, A., Reyes-Gasga, J.** In Situ X-ray Rietveld Analysis of Ni–YSZ Solid Oxide Fuel Cell Anodes During NiO Reduction in H_2 *J. Phys. D: Appl. Phys.* 2005: pp. 2276 – 2282.
9. **Ma, W., Pan, W. X., Wu, C. K.** Preliminary Investigations on Low-Pressure Laminar Plasma Spray Processing *Surface & Coatings Technology* 2005: pp. 166 – 174.
10. **Lide, D. R.** CRC Handbook of Chemistry and Physics. CRT, 1994
11. **Lazbyn'sh, A., Avots, A., Ulaste, V., Leitis, L., Shymanskaya, M.** Application of the Ortogonal Planning method for Optimization of the Synthesis of Dipyroxime *Khimiko-Farmatsevticheskii Zhurnal* 1973: pp. 38 – 41.
12. **Montgomery, D. C.** Design and Analysis of Experiments Wiley, 1998: 704 p.

Presented at the National Conference "Materials Engineering'2007" (*Kaunas, Lithuania, November 16, 2007*)